

AD 729684

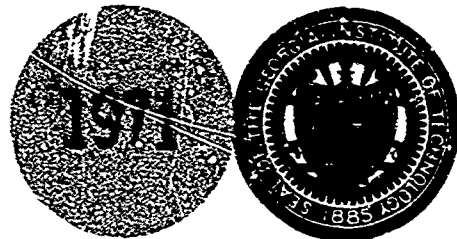
TECHNICAL REPORT NO. 1
PROJECT NO. A1231

MODELS FOR RADAR DISPLAYS

by Wayne Rivers

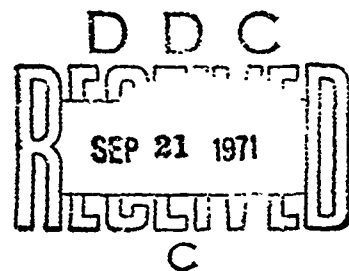
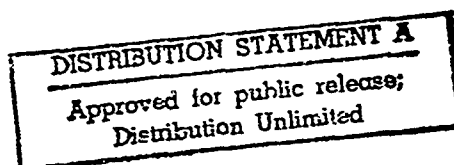
Contract No. N00024-70-C-1219
Project Serial No. S-3643, Task 12361
Department of the Navy
Naval Ship Systems Command
Washington, D. C. 20360

17 July 1971



Engineering Experiment Station
GEORGIA INSTITUTE OF TECHNOLOGY
Atlanta, Georgia

Reproduced by
NATIONAL TECHNICAL
INFORMATION SERVICE
Springfield Va 22151



45

UNCLASSIFIED

Security Classification

DOCUMENT CONTROL DATA - R & D

Security classification of title, body of abstract and indexing annotation must be entered when the overall report is classified

1. ORIGINATING ACTIVITY (Corporate author) Engineering Experiment Station Georgia Institute of Technology Atlanta, Georgia 30332		2a. REPORT SECURITY CLASSIFICATION Unclassified	
3. REPORT TITLE "Models for Radar Displays"		2b. GROUP	
4. DESCRIPTIVE NOTES (Type of report and inclusive dates) Technical Report No. 1			
5. AUTHOR(S) (First name, middle initial, last name) Wayne Rivers			
6. REPORT DATE 17 July 1971		7a. TOTAL NO OF PAGES iv + 37	7b. NO OF REFS 17
8a. CONTRACT OR GRANT NO N00024-70-C-1219		9a. ORIGINATOR'S REPORT NUMBER(S) A-1231-TR-1	
b. PROJECT NO		9b. OTHER REPORT NO(S) (Any other numbers that may be assigned this report)	
c.		d.	
10. DISTRIBUTION STATEMENT			
11. SUPPLEMENTARY NOTES Georgia Tech Project A-1231		12. SPONSORING MILITARY ACTIVITY Naval Ship Systems Command Washington, D. C. 20360	
13. ABSTRACT <p>Mathematical models are developed to describe the capability of human operators observing A, B, and PPI displays of noncoherent radars for detecting target signals in receiver noise. The models are derived from visibility data of World-War II experiments using curve-fitting techniques guided by simple physical models. The trends of performance are compatible with the predictions of detection theory, but calibration constants are assigned based upon experimentally determined human operator characteristics. Radar variables which are incorporated in the models include pulse length, receiver bandwidths, antenna beamwidth and scan rate, pulse repetition frequency, and display brightness, geometry and phosphor characteristics. Data are presented from experiments on detection of target signals in sea clutter by human operators.</p>			

DD FORM 1473 (PAGE 1)

1 NOV 65

N 0101-807-6801

UNCLASSIFIED

Security Classification

UNCLASSIFIED

Security Classification

KEY WORDS	LINK A		LINK B		LINK C	
	ROLE	WT	ROLE	WT	ROLE	WT
Experimental Data	1					
Mathematical Models	2, 8					
Performance Prediction	4					
Clutter	6					
Noise	6					
Operator	9					
Display	9					
A-Scope	9					
B-Scope	9					
Plan Position Indicator	9					
Radar	9					

DD FORM 1473 (BACK)

1 NOV 85
(PAGE 2)

UNCLASSIFIED

Security Classification

Engineering Experiment Station
Georgia Institute of Technology
Atlanta, Georgia

Technical Report No. 1

MODELS FOR RADAR DISPLAYS

by

Wayne Rivers

17 July 1971

Contract No. N00024-70-C-1219
Georgia Tech Project A-1231

Prepared for:
Department of the Navy
Naval Ship Systems Command
Washington, D. C. 20360

Contract N00024-70-C-1219
Naval Ship Systems Command
Washington, D.C. 20360

A-1231-TR-1
Engineering Experiment Station
Georgia Institute of Technology
Atlanta, Georgia 30332

MODELS FOR RADAR DISPLAYS

by

Wayne Rivers

ABSTRACT

Mathematical models are developed to describe the capability of human operators observing A, B, and PPI displays of noncoherent radars for detecting target signals in receiver noise. The models are derived from visibility data of World-War-II experiments using curve-fitting techniques guided by simple physical models. The trends of performance are compatible with the predictions of detection theory, and calibration constants are assigned based upon experimentally determined human operator characteristics. Radar variables which are incorporated in the models include pulse length, receiver bandwidth, antenna beamwidth and scan rate, pulse repetition frequency, and display brightness, geometry and phosphor characteristics. Data are presented from experiments on detection of target signals in sea clutter by human operators.

TABLE OF CONTENTS

	<u>Page</u>
I. Introduction	1
II. A-Scope Model.	3
III. PPI Model.	10
IV. Probability-of-Detection Functions	19
V. Target Exposure Time	23
VI. Detection in Sea Clutter	26
VII. Acknowledgements	32
VIII. References	33
IX. Appendix	
A. Properties of a Curve-Fitting Function	34
B. Brief Summary of FOCAL Commands and Symbols.	35

LIST OF FIGURES

	<u>Page</u>
1. Approximate probability of detection of a log-normally distributed target signal	22
2. Approximation to cumulative probability of detection of log-normally distributed signals for 30 and 200 independent antenna scans	25
3. Probability of spike signal being above threshold received power	29

LIST OF TABLES

	<u>Page</u>
I. Input Variables for A-Scope Model	5
II. Intermediate Variables of the A-Scope Equations	6
III. A-Scope Model Equations	7
IV. A-Scope Model Program	8
V. Comparison of A-Scope Data with Model Calculations.	9
VI. Input Variables for PPI Model	11
VII. Intermediate Variables of PPI Model	12
VIII. PPI Model Equations	13
IX. Program for PPI Display Model	15
X. Comparison of PPI Data with Model Calculations.	16
XI. Median Clutter Spike Cross Sections	30
XII. Selected FOCAL Commands and Symbols	36

I. INTRODUCTION

The detection of radar signals is implemented using human operators viewing displays which are either deflection or intensity modulated by the received signal. The properties of these displays were studied extensively during World War II and sporadically since that time in investigations to describe the dependences of the minimum detectable signal-to-noise ratio on the numerous radar variables and parameters. Attempts to build mathematical functions to represent these dependences were made by Haeff [1] for the A-Scope and Payne-Scott [2] for the PPI display, but other investigators have ignored the question of a comprehensive model.

In the present study, the models of Haeff and Payne-Scott and the contributions of others since have been reviewed, and revised functions have been derived to describe the performance of human operators viewing real radar displays of the A and PPI types under the following assumptions:

- (1) Adequate time is provided for the operator to scan the area in which signals are presented.
- (2) The target signal is non-fluctuating in a background of receiver noise.
- (3) The operator is not handicapped by long-term fatigue effects or other distractions.
- (4) The minimum detectable signal-to-noise ratio corresponds to a probability of detection of 0.5 within a basic time interval of a single scan or phosphor decay-time constant, whichever is longer.

In the following chapters the A-Scope and PPI display are treated by identifying the pertinent input variables, by presenting an algorithm expressing the minimum detectable signal-to-noise ratio as a function of the input variables, and by discussing the physical significance of the various factors of the function. Validation of the algorithms is offered by referencing specific experimental work to which the function's parameters are adjusted. The domains over which the algorithms are considered valid are identified in the respective chapters. The accuracy of the equations and

parameters is such that the fit to the data is comparable to the spread of the data points (about ± 1.5 dB) except at a few combinations of parameters.

The output of the display models is a minimum-detectable signal-to-noise ratio for a probability of detection of a pulsed noncoherent signal in noise on a single antenna scan of 0.5 or 0.9 as appropriate. The conditions of applicability are those associated with the use of the term "detectability" which implies that a limited amount of eye scanning is required, as contrasted with the term "visibility," in which foreknowledge of the location of the pulse is available to the observer. However, these models predict performance which will be better, in general, than in real situations in which operators' efficiency is reduced by boredom, fatigue, and distractions. No attempt is made here to model these effects or those of backgrounds including interference or confusing targets. References 3 and 4 contain information on these topics, but the source information is not considered reliable enough to include in a model at this time.

Included in this report are continuous-function models applicable to A, PPI, and B displays, discussions of probability of detection as a function of signal-to-noise ratio and of target exposure time. Also included are simple computer programs for the equations in FOCAL* language. A simple model for detection in a clutter-spike background is discussed based on experimental data.

*FOCAL (FORMula CALculator) is a Trade Mark of the Digital Equipment Corporation.

II. A-SCOPE MODEL

Outstanding work in characterizing the performance of humans observing A-scopes was performed in Group 44 of the Radiation Laboratory in World War II and reported by Haeff [1] and Lawson and Uhlenbeck [5]. The former reference offers a simple mathematical expression for the performance, whereas the latter reference collects a more complete group of studies of dependences of performance on radar variables.

The model proposed here is shown in Tables I through IV. An additional assumption for the A-scope not mentioned in the introduction is:

(5) Adequate display brightness and contrast in room light is offered.

The model is believed to be applicable over the following range of variables:

P.R.F.	$12 < f_r < 3000 \text{ Hz}$
Pulse-length x bandwidth	$0.15 < B\tau < 20$
Display duration	$0.01 < T_D < 60 \text{ sec}$
No. of cells displayed	$2 < N_s < 60$
Angle subtended by pulse	$2 \times 10^{-5} < \alpha < 0.03 \text{ radians}$

The agreement with the experimental data of Haeff [1] and Lawson and Uhlenbeck [5] is illustrated by Table V and appears to be typically within about ± 1.5 dB. Calibration of the constant C_A was made using the data of Figures 8.18, 8.23 and 8.27 of Reference 3.

Two dependences which have been studied were not included in the model, because under normal conditions they result in negligible effect on visibility. First, the product of video bandwidth times pulse length was found to have no measurable effect on visibility over a range of 0.1 to 10 [3]. Second, the amount of deflection of the spot produced by average noise was found to de-

grade the visibility if it was less than about 0.5 mm (≈ 1.5 mr) but no improvement was seen for deflections above that value. It should be possible in all practical situations to provide a deflection of a few milliradians at the eye.

It was stated by Lawson that display brightness was not an important variable in determining A-scope visibility, provided the observer "can see the trace clearly." This result is potentially in contradiction with the Blackwell contrast model [6] which implies that brightness should be an important factor at levels less than about 10 foot-Lamberts. Trace brightness appears to enter the A-scope model by determining the critical repetition rate, f_c . A brighter trace should improve the contrast sensitivity of the eye and raise f_c , the repetition frequency at which the noise background is no longer granular to the eye. The value of f_c chosen here is that found empirically by Lawson. No evidence is shown that the dependence of f_c on brightness was studied.

Table I

Input Variables for A-Scope Model

<u>Symbol</u>	<u>Units</u>	<u>FOCAL Symbol</u>	<u>Definition</u>
B	MHz	BW	Bandwidth of Receiver (IF)
τ	μsec	TP	Transmitted Pulse Length
R_D	nmi	RD	Displayed Range Interval
D_o	in	OD	Distance of Eye from Scope
S	RPM	SC	Antenna Scan Rate
θ_a	Deg	BM	Azimuth Antenna Beamwidth (3-dB one-way)
f_r	Hz	RP	Pulse Repetition Frequency
D	in	LD	Display Trace Length

Table II

Intermediate Variables of the A-Scope Equations

<u>Symbol</u>	<u>FOCAL Symbol</u>	<u>Definition</u>
G_{BandA}	GB	Receiver bandpass filter factor
s	SM	Display sweep rate (in/ms)
α	AL	Angle subtended at eye by pulse on display (rad)
α_c	--	A critical angle
G_{Sweep}	GS	Factor related to apparent size of pulse
f_c	--	A critical prf at which the noise is uniform in density to the eye
G_{RepA}	GR	Integration factor
T_D	TD	Time pulses are near maximum height as beam scans past target
G_{Time}	GT	Factor for finite display time
N_s	NS	Number of radar cells displayed
G_{Cells}	GC	Factor of improvement for few cells monitored
C_A	CA	Calibration factor
P_{min}/P_n	(LP in dB)	Minimum detectable target signal-to-average-noise ratio referred to receiver input (noise in bandwidth B)

Table III
A-Scope Model Equations

$$1. \quad G_{\text{BandA}} = \left(1 + \frac{1}{B_T}\right)^2$$

$$2. \quad s = \frac{D}{12.36 R_D}$$

$$\alpha = \frac{s\tau}{D_o}$$

$$\alpha_c = 0.004 \text{ rad}$$

$$G_{\text{Sweep}} = 0.63 \left[\frac{1 + (\alpha/\alpha_c)^2}{\alpha/\alpha_c} \right]^{1/3}$$

$$3. \quad f_c = 2 \text{ kHz}$$

$$G_{\text{RepA}} = \left[\frac{1 + f_r/f_c}{f_r/f_c} \right]^{1/2}$$

$$4. \quad T_D = \frac{\theta_h}{12 \text{ s}}$$

$$T_c = 8 \text{ sec}$$

$$G_{\text{Time}} = \frac{1 + (T_D/T_c)^{2/3}}{(T_D/T_c)^{2/3}}$$

$$5. \quad N_s = \frac{D}{s\tau}$$

$$G_{\text{Cells}} = \frac{N_s}{2 + N_s}$$

$$6. \quad C_A = \begin{cases} 0.017 & \text{for } P_D = 0.9 \\ 0.011 & \text{for } P_D = 0.5 \end{cases}$$

$$\frac{P_{\min}}{P_{1t}} = C_A \cdot G_{\text{BandA}} \cdot G_{\text{Sweep}} \cdot G_{\text{RepA}} \cdot G_{\text{Time}} \cdot G_{\text{Cells}}$$

Table IV. A-Scope Model Program

C-FOCAL S 2/71

01.02 C A-SCOPE MODEL; TO INPUT VARIABLES G 1.30

01.10 S CA=.017

01.20 G 2.10

01.30 A ?BW TP RP BM SC RD LD OD ?

02.10 S GB=(1+1/BW/TP)+2

03.10 S SM=LD/12.35/RD

03.20 S AL=SM*TP/OD

03.30 S GS=.63*FEXP(FLOG(4E-3*(1+AL/4E-3)+2)/AL)/3)

04.10 S GR=FSQT(2E3*(1+RP/2E3)/RP)

05.10 S TD=BM/12/SC

05.20 S GT=FEXP(2*FLOG(TD/8)/3)

05.30 S GT=(1+GT)/GT

06.10 S NS=LD/SM/TP

06.20 S GC=NS/(2+NS)

07.10 S LP=4.34*FLOG(CA*GB*GS*GR*GT*GC)

08.20 T I 14.02, ?LP ?

*

Table V. Comparison of A-scope Data with Model Calculations

$D_o = 304.8 \text{ mm}$
 $D = 76.2 \text{ mm}$

BT	f_r (Hz)	T_D (sec)	sT	P_{min}/P_n (dB) ¹		Diff (dB)
				Calculated	Data ²	
1.2	200	0.043	0.05	+10.7	+10.2	+0.5
			0.25	+ 8.4	+ 7.7	+0.7
			1.5	+ 6.9	+ 7.2	-0.3
1.2	200	3	0.005	+ 3.4	+ 3.7	-0.3
			0.05	+ 0.1	- 0.3	+0.4
			0.7	- 3.4	- 3.8	+0.4
			2	- 3.6	- 3.8	+0.2
			9	- 2.6	- 2.3	-0.3
13	12	3	1.7	- 2.4	- 2.1	-0.3
	200			- 8.3	- 7.6	-0.7
	3000			+12.4	-13.1	+0.7
0.18	12	3	1.7	+13.3	+13.4	-0.1
	200			- 7.4	+ 7.9	-0.5
	3000			+ 3.3	+ 3.4	-0.1
1.1	12	3	1.7	+ 2.6	+ 2.1	+0.5
	200			- 3.3	- 3.4	+0.1
	3000			- 7.4	- 7.4	0
(1.2) ³	200	0.04	0.25	+10.9	+10.3 ⁴	+0.6
		0.5		4.1	5.2	-1.1
		4		- 0.5	1.2	-1.7
		60		- 3.6	- 1.8	-1.8
(1.2) ³	3200	0.012	1.6	+ 6.4	+ 6.2 ⁴	+0.2
		0.12		- 0.1	- 3.1	+3.0
		1.5		- 6.4	- 7.8	+1.4
		15		-10.3	-11.1	+0.8

Av. $0.1 \pm 0.9 \text{ dB rms}$

- Note: 1. Criterion of $P_D = 0.9$.
2. Data from Reference 5, Figures 8-18, 8-23, and 8-27 have been adjusted by subtracting $10 \log (BT)$.
3. Assumed value.
4. Average of P-1 and P-7 data from Reference 5, Figures 8-27.

III. PPI MODEL

The work of Payne-Scott [2] of the Australian CSIR on the performance of humans viewing PPI displays is outstanding for its comprehensiveness and physical insight, and it is the principal basis for the model presented here. The Payne-Scott work is so complete that no work on PPI displays since published can be compared with it without assuming values for missing important variables.

The model is presented in Tables VI through IX. It is applicable over the following range of variables:

Ratio of pulse length to spot size	$0.1 < \frac{t_s}{d} < 10$
Pulse length and bandwidth	$0.1 < B\tau < 20$
Screen brightness	$0.001 < I < 100$ ft Lamberts
Antenna scan rate	$1 < S < 100$ rpm
Azimuth beamwidth	$1 < \theta_h < 12$ deg
P.R.F.	$40 < f_r < 4000$ Hz

It is not implied that the model is not valid outside these limits, but only that it has not been adequately compared with data outside them. The model is derived from that of Payne-Scott by making two changes. The "hard" corners of the model have been replaced by "soft" ones allowing the use of continuous functions for representation, and a liminal-contrast model based on the newer data of Blackwell [6] has been used. The use of the Blackwell model results in underestimation of P_{min}/P_n and necessitates the introduction of the calibration constant, C_p .

The model equations and parameters were validated using Payne-Scott's data of Figures 7.2, 7.3, 7.4, and 7.5 of Reference 2. The values of variables used by Payne-Scott but not studied were:

$$\begin{aligned}
D &= 2.25 \text{ in} \\
R &= 0.45 R_D \\
D_o &= 15 \text{ in} \\
k_1 &= 3 \\
k_1 &= 2 \\
\left. \begin{aligned} a &= 0.15 \text{ sec}^{-1} \\ b &= 1.2 \end{aligned} \right\} &\text{for P7 phosphor} \\
I &= 0.126 \text{ ft-Lambert} = 0.04 \text{ ft-candle} \\
d &= 0.024 \text{ in}
\end{aligned}$$

The value of the calibration constant C_p was adjusted to give minimum difference between the Payne-Scott data and the model prediction. The result, shown in Table X, is a maximum difference of 3.4 dB between the two (which is slightly greater than the internal variation of the Payne-Scott data) and quantitative agreement between the two with respect to location of break points and to slopes of asymptotes.

The liminal-contrast model for the eye (G_{Contr}) was designed to fit the family of curves of Figure 16 of Reference 6, which applies to long exposure of the target to take advantage of eye scanning. The data of Blackwell's Figure 11, which apply to a 6-second exposure of the target, have the same shape as for long exposure but correspond to a constant of 2.3 (instead of 1.27) in the formula for G_{Contr} in Table V. The necessity to introduce C_p is hypothesized to be required because (a) the Payne-Scott experiment allowed more possible positions for the target than Blackwell's, and (b) Payne Scott's target was soft-edged and generally not symmetrical, whereas Blackwell's was round with an abrupt-contrast perimeter. The data of Schade [7] suggest that the liminal-contrast sensitivity of the eye is strongly adversely affected by the "softness" of target contour, especially of larger targets.

The PPI model can be used for describing the performance of a B-display by making two changes. In Sections 3 and 5 of Table VIII, R is replaced by R_D , and the formulae for N_s , G_{Exc} , and h_s are changed by setting $D = W/2\pi$ where W is the azimuth width of the display. The formula for s is not changed, but in it, D is the range dimension of the display.

Table VI

Input Variables for PPI Model

<u>Symbol</u>	<u>Units</u>	<u>FOCAL Symbol</u>	<u>Definition</u>
B	MHz	BW	Bandwidth of Receiver (IF)
τ	μs	TP	Pulse Length
θ_a	deg	BM	Azimuth Antenna Beamwidth
L	in	LD	Length of Display Trace
d	in	SP	Diameter of Beam Spot
D_o	in	OD	Distance of Observer's Eye from Screen
R	nmi	RA	Range to Target
R_D	nmi	RD	Display Range
f_r	Hz	RP	Pulse Repetition Rate
S	rpm	SC	Antenna Scan Rate
k_1		K1	C-R-T Grid-Transfer-Law Exponent
k_2		K2	$\left\{ \begin{array}{l} = 1 \text{ for square-law detector} \\ = 2 \text{ for linear detector} \end{array} \right.$
a	s^{-1}	DE	Decay Rate of C-R-T Phosphor
b		QB	Exponent of Decay Factor
I	ft-Lambert	IN	Brightness of Noise Background on C-R-T Screen
P_{\min}/P_n	dB	LP	Minimum Detectable Target-Signal-to-Average-Noise Ratio Referred to Receiver Input

Table VII

Intermediate Variables of PPI Model

Symbol	FOCAL Symbol	Definition
G_{BandP}	GB	Response factor of Receiver/Filter
G_{Trans}	(T	Non-linear response factor of envelope detector and C-R-T grid
G_{Exc}	GE	Excitation factor of a beam spot produced by signal pulses
G_{Contr}	GC	Contrast sensitivity of the eye
G_{RepP}	GR	Integration factor for noise pulses
i_{min}/P_n	LP(in dB)	Minimum-detectable target-signal-to-average-noise ratio referred to receiver input
s	SM	Sweep rate of beam (in/ μ s)
h_s	SA	Cell-size/spot-size factor
ϕ_s	SE(01)	Solid angle of beam spot at eye (ster)
ϕ	SE(00)	Solid angle of radar cell at eye (ster)
ϕ_c	—	A critical solid angle of eye contrast sensitivity
q	QE	A "softness" exponent
n_s	NS	Number of noise pulses integrated in one beam spot in one scan
n	NN	Total number of noise pulses integrated per spot
C_P	CP	A calibration constant

Table VIII

PPI Model Equations

$$1. \quad G_{\text{BandP}} = \frac{1}{\left(1 - e^{-2B\tau}\right)^2}$$

$$2. \quad G_{\text{Trans}} = \frac{k_2}{k_1}$$

$$3. \quad s = \frac{D}{R_D \cdot 12.36}$$

$$h_s = \left[\left\{ 1 + \left(\frac{\tau_s}{d} \right)^2 \right\} \left\{ 1 + \left(\frac{\theta_a R_D \pi}{d R_D 180} \right)^2 \right\} \right]^{1/2}$$

$$G_{\text{Exc}} = h_s \left\{ \frac{1}{\frac{\tau_s}{d} \frac{\theta_a R_D \pi}{d R_D 180}} \right\}$$

$$4. \quad \phi = h_s \cdot \frac{\pi}{4} \frac{d^2}{D_o^2}$$

$$\phi_c = 5 \times 10^{-6} \frac{1 + I^{0.55}}{I^{0.55}}$$

$$q = (0.08 \ln \phi_c)^2$$

$$G_{\text{Contr}} = 1.27 \phi_c^{1/2} \frac{\left(1 + \left(\frac{\phi}{\phi_c} \right)^q \right)^{1/q}}{\frac{\phi}{\phi_c}} = G_{\text{Contr}}(\phi, I)$$

Table VIII (continued)

$$\begin{aligned}
 5. \quad \phi_s &= \frac{\pi}{4} \frac{d^2}{D_o^2} \left[1 + \left(\frac{s}{2Bd} \right)^2 \right]^{1/2} \\
 n_s &= \frac{7.5 f_r d R_D}{s D R} \left[1 + \left(\frac{2Bd}{s} \right)^2 \right]^{1/2} \\
 n &= n_s \frac{1 + \left(1 + \frac{60a}{S} \right)^{-b}}{1 - \left(1 + \frac{60a}{S} \right)^{-b}} \\
 G_{RepP} &= \left[1 + \frac{1}{n \cdot G_{Contr}^2(\phi_s, 1) \cdot G_{Trans}^2} \right]^{1/2} \\
 6. \quad C_P &= 5.2 \\
 P_{min}/P_n &= C_P \cdot G_{BandP} \cdot G_{Trans} \cdot G_{Exc} \cdot G_{RepP} \cdot G_{Contr}
 \end{aligned}$$

Table IX. Program for PPI Display Model

C-FOCAL S 2/71

```

01.01 C PPI MODEL. TO INPUT VARIABLES, G 1.22.
01.10 S PI=3.14159
01.20 S CP=5.2
01.21 G 1.30
01.22 A ? BW TP TA LD SP OD RD RA RP SC KI K2 DE QB IN ?
01.23 G 1.1
01.30 F RA=RD/10, RD/10, RD; D 2; D 1.40
01.35 QUIT
01.40 T ! 15.02, ?RD, RA, LP ?

02.10 S GB=1/(1-FEXP(-2*BW*TP))+2
02.20 S GT=K2/K1
02.31 S SM=LD/RD/12.35
02.32 S T1=TP*SM/SP
02.33 S T2=LD*TA*PI*RA/180/SP/RD
02.34 S SA=FSQT((1+T1*T1)*(1+T2*T2))
02.35 S GE=SA/T1/T2
02.37 S SE(00)=SA*PI*((SP/OD)+2)/4
02.39 S J=0; D 3
02.41 S KR=FSQT(1+(2*BW*SP/SM)+2)
02.43 S SE(01)=SP+2*PI*FSQT(1+(SM/2/BW/SP)+2)/4/OD+2
02.55 S NS=KR*7.5*RP*SP*RD/SC/LD/RA
02.57 S T3=FEXP(FLOG(1+60*DE/SC)*(-QB))
02.59 S NN=NS*(1+T3)/(1-T3)
02.61 S J=1; D 3.4; D 3.5
02.62 S GR=FSQT(1+1/NN/GC(01)+2/GT+2)
02.70 D 4

03.10 S T4=FEXP(.55*FLOG(IN))
03.20 S ST=5E-6*(1+T4)/T4
03.30 S QE=(.08*FLOG(ST))+2
03.40 S GC(J)=FEXP(FLOG(1+FEXP(QE*FLOG(SE(J)/ST)))/QE)
03.50 S GC(J)=GC(J)*1.27*ST*FSQT(ST)/SE(J)

04.10 S LP =10 *FLOG(GB*GT*GE*GC(00)*GR*CP)/FLOG(10)
*
```


Table X. Comparison of PPI Data with Model Calculations

$\tau = 1 \mu s$
 $R = 0.45 R_D$
 $D_0 = 15 \text{ in}$
 $d = 0.024$
 $I = 0.12 \text{ ft L}$

$k_1 = 3$
 $k_2 = 2$
 $a^2 = 0.15$
 $b = 1.2$
 $L = 2 \text{ in}$

$\frac{\tau s}{d}$	$f_r \text{ (Hz)}$	B_T	$S \text{ (rpm)}$	$\theta_a \text{ (Deg)}$	$P_{min}/P_n \text{ (dB)}^1$		Diff (dB)
					Calculated	Data ²	
0.1	1600	1.5	4	4	+ 0.6	- 0	+0.6
1.0					- 7.5	- 8	+0.5
10					- 8.1	- 9.5	+1.4
0.1	100	1.7	4	4	+ 2.3	+ 2	+0.3
1					- 3.2	- 3	-0.2
10					- 2.7	- 4	+1.3
0.1	200	1	4	4	+ 3	- 3.5	-0.5
1					- 2.5	- 1.5	-1
10					- 1.7	- 3	+1.3
7.2	40	1.5	4	4	- 0.7	- 2	+1.3
	400				- 5.6	- 7	+1.4
	4000				-10.3	-12	+1.7
0.45	40	2	4	4	- 0.3	+ 1.5	-1.8
	400				- 4.4	- 3	-1.4
	4000				- 5.0	- 5.5	-0.5
0.1	40	1.5	4	4	+ 4.0	+ 5	-1.0
	400				+ 1.2	+ 1	+0.2
	4000				+ 0.5	+ 1	-0.5
0.93	1600	13	4	2	- 6.8	- 6.5	-0.3
				4	- 9.1	- 8.5	-0.6
				8	-11.1	-10.5	-0.6
7.2	100	1.5	4	2	- 1.0	+ 0.5	-1.5
				4	- 2.6	- 1.5	-1.1
				8	- 3.8	- 3	-0.8
7.2	100	1.5	64	2	+ 0.7	+ 3	-2.3
				4	- 1.0	+ 0.5	-1.5
				8	- 2.1	- 1	-1.1

Table X. Comparison of PPI Data with
Model Calculations (Continued)

$\frac{\tau_s}{d}$	f_r (Hz)	$B\tau$	S (rpm)	θ_a (Deg)	P_{min}/P_n (dB) ¹		$Diff$ (dB)
					Calculated	Data ²	
7.2	400	1.5	1	4	- 7.9	- 7	-0.9
			4		- 5.6	- 6	+0.4
			10		- 4.7	- 6	+1.3
			50		- 4.0	- 5	+1.0
0.1	1600	1.5	1	4	+ 0.4	- 3	+3.4
			4		+ 0.6	- 1	+1.6
			10		+ 0.7	- 1	+1.7
			50		+ 0.8	0	+0.8

Average 0.1 ± 1.3 dB

- Notes: 1. Criterion $P_D = 0.5$.
2. Data from Reference 2

IV. PROBABILITY-OF-DETECTION FUNCTIONS

The display models presented in the two preceding chapters are designed to predict the target-signal-to-noise ratio which would result in a 0.5 probability of detection. However, other probability levels are of interest, and the function $P_D(X)$, where $X = 10 \log (P_{\text{sig}}/P_n)$, is the representation sought. Such functions have been calculated in abundance for the case of the automatic detector, consisting of an ideal envelope integrator followed by a threshold [8, 9, 10]. The functions have been measured for a human observing an intensity-modulated display by Tucker [11]. It is of interest to compare the two cases. Because of the scatter in the experimental data, the only information about the shape of the function that it is reasonable to extract is the slope near $P_D = 0.5$. For example, Tucker's data for $N = 28$ pulses displayed imply a slope for dP/dX of about 0.2 dB^{-1} whereas the calculations of DiFranco and Rubin show a corresponding slope of 0.23 dB^{-1} for $N = 30$ and a false alarm number, n' , of 10^{3*} ; which is close to that recommended by Skolnik [12] as best fitting the data of Tucker. Thus the two cases are in good agreement with respect to the width of the curves. In addition the curves for the operator tend to increase in width (decrease in slope) as N increases. This trend is followed for the automatic detector only if the number of pulses between false alarms is held constant. If the probability of false alarm per unit time is held constant, the trend is for the slope to increase with increasing N . Thus one concludes that the human can operate with a lower effective threshold setting than the automatic detector with constant false-alarm probability.

It is concluded that the automatic-detector probability-of-detection functions are an adequate representation of human performance for a false-alarm rate of $10^{-4.35}$ per pulse [12], provided the signal-to-noise ratio corresponding to $P_D = 0.5$ is adjusted to be that predicted by the appropriate model.

For a nonfluctuating signal, the probability of detection is related to signal-to-noise ratio approximately as follows:

* n' is the reciprocal of the false-alarm probability.

$$P_D \approx \frac{\exp(0.45 X \ln 10)}{1 + \exp(0.45 X \ln 10)} \quad (1)$$

This approximation is derived from the curves of Reference 10 for 30 integrated pulses and a false-alarm number of 10^3 .

The shape of the probability-of-detection function is not a strong function of either number of pulses integrated or false-alarm number, provided one does not require accuracy of the representation in (1) for either very small or very large values of P_D .

The relationship in (1), which is for a nonfluctuating target in a background of noise, can be considered to be a conditional probability, and the rules relating conditional and joint probabilities can be used to derive an expression for P_D for fluctuating targets, provided their signal-strength distributions are known. Call the probability of detection for a fluctuating target P_V , and let the density function of signal strength be given as $p(X)$ in terms of the normalized variable X . Then

$$P_V(X_i) = \int_x P_D(X) p(X|X_i) dX, \quad (2)$$

where X_i represents parameters of the distribution. For example, let a target be log-normally distributed with median X_0 and standard deviation σ_X , so that

$$P_V(X) dX = \frac{1}{\sqrt{2\pi} \sigma_X} \exp \left\{ -\frac{(X - X_0)^2}{2\sigma_X^2} \right\} dX, \quad (3)$$

where X_0 and σ_X are in dB.

Then,

$$P_V(X_0, \sigma_X) = \int_{-\infty}^{\infty} \frac{\exp \left[-\frac{(X - X_0)^2}{2\sigma_X^2} \right]}{\sqrt{2\pi} \sigma_X (1 + \exp[-0.45 X \ln 10])} dX \quad (4)$$

This expression has been evaluated numerically for $\sigma_X = 0, 3$, and 6 dB and the results are plotted in Figure 1. It is seen that the width of the P_V function increases as σ_X increases.

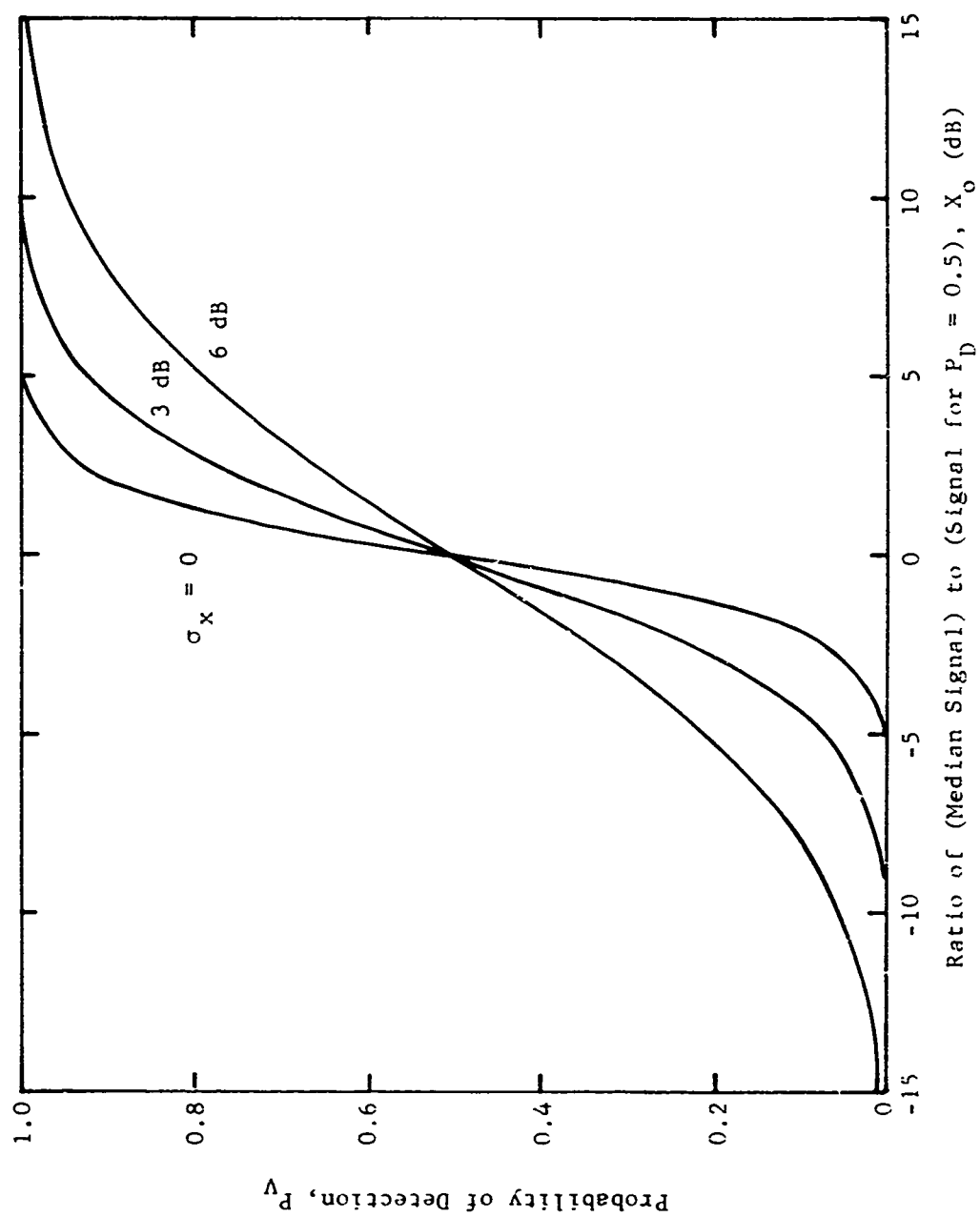


Figure 1. Approximate probability of detection of a log-normally distributed target signal.

V. TARGET-SIGNAL EXPOSURE TIME

Both the display models presented here predict the detectability of a target signal in receiver noise with limited eye scanning required. That is, by detectability is meant the signal which can just be detected provided that the operator is operating at maximum efficiency and has adequate time to search the area displayed and utilize the foveal sensitivity of the eye. Thus detectability represents an intermediate ideal that is achievable under many circumstances, but in many other situations an operator's performance may be degraded. If exposure time of the target signal is too short for effective eye scanning, then the minimum detectable signal may be limited by the off-axis sensitivity of the eye. This sensitivity function is related to the foveal sensitivity, $(\delta I/I)_{\min}$ by [13]

$$\left(\frac{\delta I}{I}\right)_{\text{off axis}} = \left(\frac{\delta I}{I}\right)_{\min} \cdot \exp \{+0.202 \theta\} , \quad (5)$$

where θ is the angle in degrees of a line to the target spot from the foveal axis. Note that this function implies that an increase in contrast of 10 dB is required at an angle of 11.4 degrees off the foveal axis, which is the half-angle subtended by a 5-inch display at 12 inches from the eye. The use of Equation 2 is properly that of an upper bound to eye sensitivity degradation, unless a detailed eye scanning model can be postulated.

The detectability models are to be interpreted as applying to a single integration period defined by a single scan or a few scans integrated by the phosphor. If a target signal is exposed for a long time spanning many phosphor integration periods, the performance of an operator should improve. However, the appropriate quantitative means of predicting the improvement for the case of radar displays is not clear. Swets [14], in a generalized detection experiment (aural), offers data to distinguish between two prominent models of improvement. In one mode the operator is presumed to integrate the signals from M events so that improvement occurs at the rate of $M^{1/2}$ to $M^{2/3}$. In the

other mode the display storage intervals are presumed to be independent events for the operator so that this law holds for cumulative probability of detection:

$$P_C = 1 - (1 - P_D)^M, \quad (6)$$

where P_D is the single-event probability of detection. Swets' data imply that for long exposure times the operator behaves typically as if the individual events are independent of each other and no integration is performed by him. This has not been verified for radar operators, but it is tentatively appropriate to use Equation 6 for predicting cumulative probability of detection by humans for repeated detection opportunities spaced by more than about 10 sec.

Equation 6 can be more easily evaluated in the form

$$P_C = 1 - \exp \{M \ln (1 - P_D)\} . \quad (7)$$

If P_D in Equation 7 is set equal to P_V of Equation 4, cumulative distributions of detection probability result for various log-normally distributed targets. Curves are plotted in Figure 2 for $\sigma_x = 0, 3, \text{ and } 6 \text{ dB}$ and values of 30 and 200 for M , the number of independent radar scans. It is seen that the increased width of P_D is retained in P_C , the cumulative probability, and that a given overall probability of detection is achieved with lower median signal levels for wider distributed signals.

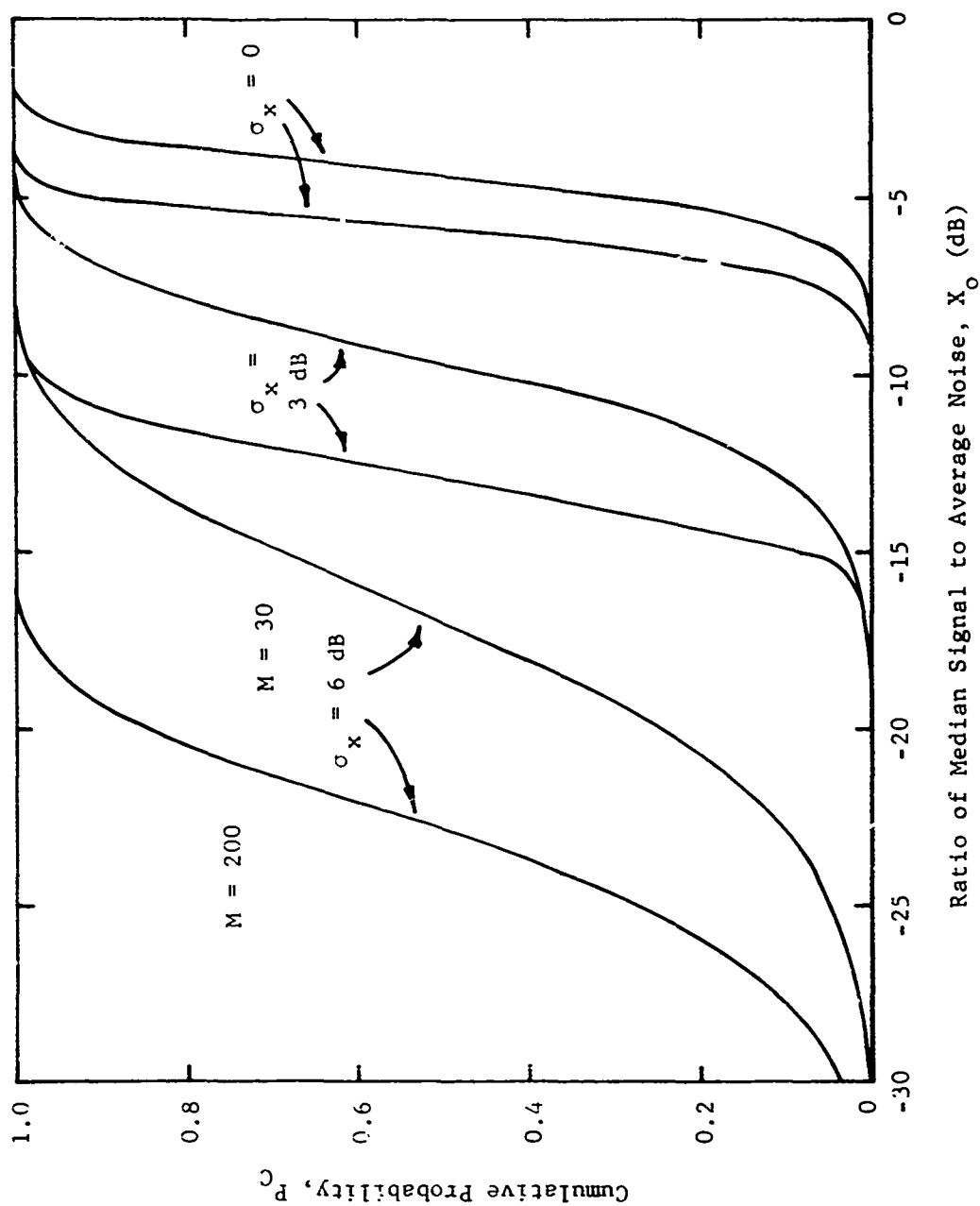


Figure 2. Approximation to cumulative probability of detection of log-normally distributed signals for 30 and 200 independent antenna scans.

VI. DETECTION IN SEA CLUTTER

Radar sea return forms a background, against which target signals are detected, that has strikingly different properties from receiver noise. The amplitude distribution of sea return is wider in dynamic range than receiver noise, and clutter signals are correlated in space and time over longer intervals, which are related to the physical wave processes rather than circuit bandwidth. Both the distribution and correlation properties adversely affect the efficiency of human radar-display observers, in addition to the simple factor of raising the average background against which target signals are presented above that of noise. Although the statistical properties of sea return are known approximately [15, 16, 17], the effects on operator performance have been described only in qualitative ways. In this chapter, one mode of behavior of an operator performing detections against a sea-clutter background is described along with a physical model justifying his behavior.

Qualitative descriptions of sea clutter since World War II have referred to its "spiky" nature, which reflects the high-energy tail of its distribution as well as its temporal and spatial correlation properties. When clutter is not considered to be spiky, it is said to be "well developed." Some conditions under which the two extreme states tend to be seen are:

Spiky Clutter: with horizontal polarization, with
 low wind speeds with swell, at low
 grazing angles.

Well-Developed Clutter: with vertical polarization, with
 high wind speeds, with very long
 pulse lengths or wide beamwidths,
 at high grazing angles.

The spike returns are presumed to result from some combination of non-uniform distribution and features of the gross surface contour [e.g., see Reference 17]

When sea return is well developed, the clutter is spatially more homogeneous than when spiky and it tends to fluctuate more rapidly. Depending on antenna scan rates, wavelength, cell size, and sea conditions, ratios of minimum-detectable target signal to average background level can be as small for homogeneous clutter as about 2 dB above the corresponding ratio for noise. However, in the spiky cases, minimum detectable ratios can be much higher than for a noise background. Therefore of the two conditions, the spiky one produces the most serious system degradation, is the least well bounded, and is the most troublesome in attempts to predict system performance with realism. In addition, most of the radar volume of interest in sea-search situations is contaminated by spiky rather than well-developed clutter.

A search for useful ways to characterize clutter spikes has been frustrating. This is because the spike is a transient phenomenon whose location in time, range, and azimuth is random, so that direct observation of a spike is difficult with the usual techniques of radar instrumentation. An important clue to one property of spikes came from a relatively crude but effective technique of observation. Systematic description of the dependences of clutter levels on various radar and environmental parameters has been carried on by many observers. In the absence of elaborate instruments it has been found that a useful measurable of clutter levels is the "average of peaks" observed by eye on an A-scope display. Its use dates from the period when the A-scope was the only quantitative instrument for wideband video observations and when envelope detectors of only limited dynamic range (linear or square law) were available. The average, median, or mode of a signal is difficult to estimate with such a detector, but the peaks are obvious. An interesting property of this "average-of-peaks" measurable is that it is fairly reproducible between successive measurements by a given observer and between different observers, and this property of reproducibility has led

to extensive use by some observers in recent times*. It was postulated that for this reliability to exist the clutter must have a well-defined high-energy boundary, which would imply a well-defined cross section for clutter spikes.

The above hypothesis was checked with an experiment in which photographs were taken of the PPI display of a high-power S-band radar under conditions of low wind (~5 kts) and substantial swell. The display was adjusted for high video gain and bias more negative than cut off so that clutter appeared as white spots on a black background. Photographs were taken of single antenna scans for different receiver gain settings from maximum (where noise could be seen) to minimum (where only strong target signals were visible) in about 5 dB steps. The number of clutter spikes (white spots) was counted in an area 45 degrees wide by 40% of displayed range centered at 0.625 times the displayed range, and that number was divided by the number of radar cells in the area (1700 to 5100 depending on displayed range) to form an estimate of false-alarm probability, P_F . The logarithm of P_F is plotted in Figure 3 against the display threshold in dBm of received power for several sequences of photographs. The result is a set of curves with plateaus of $\log P_F$ for low-power threshold regions but which drop abruptly as the threshold is increased through a certain value, which is different for different displayed ranges. The interpretation is that the radar cross section of spikes is well defined, so that the number is constant, independent of threshold until it approaches the spike level. It appears that most of the spikes in a given sample have cross sections within about ± 3 dB of the median. Using the constant for the radar of -18 dBm received power from a target of 1 m^2 cross section at 1 nmi, the median spike cross sections were calculated and are shown in Table XI.

*e.g., F. B. Dyer, Georgia Institute of Technology, and R. Hess, Airtronics, Inc.

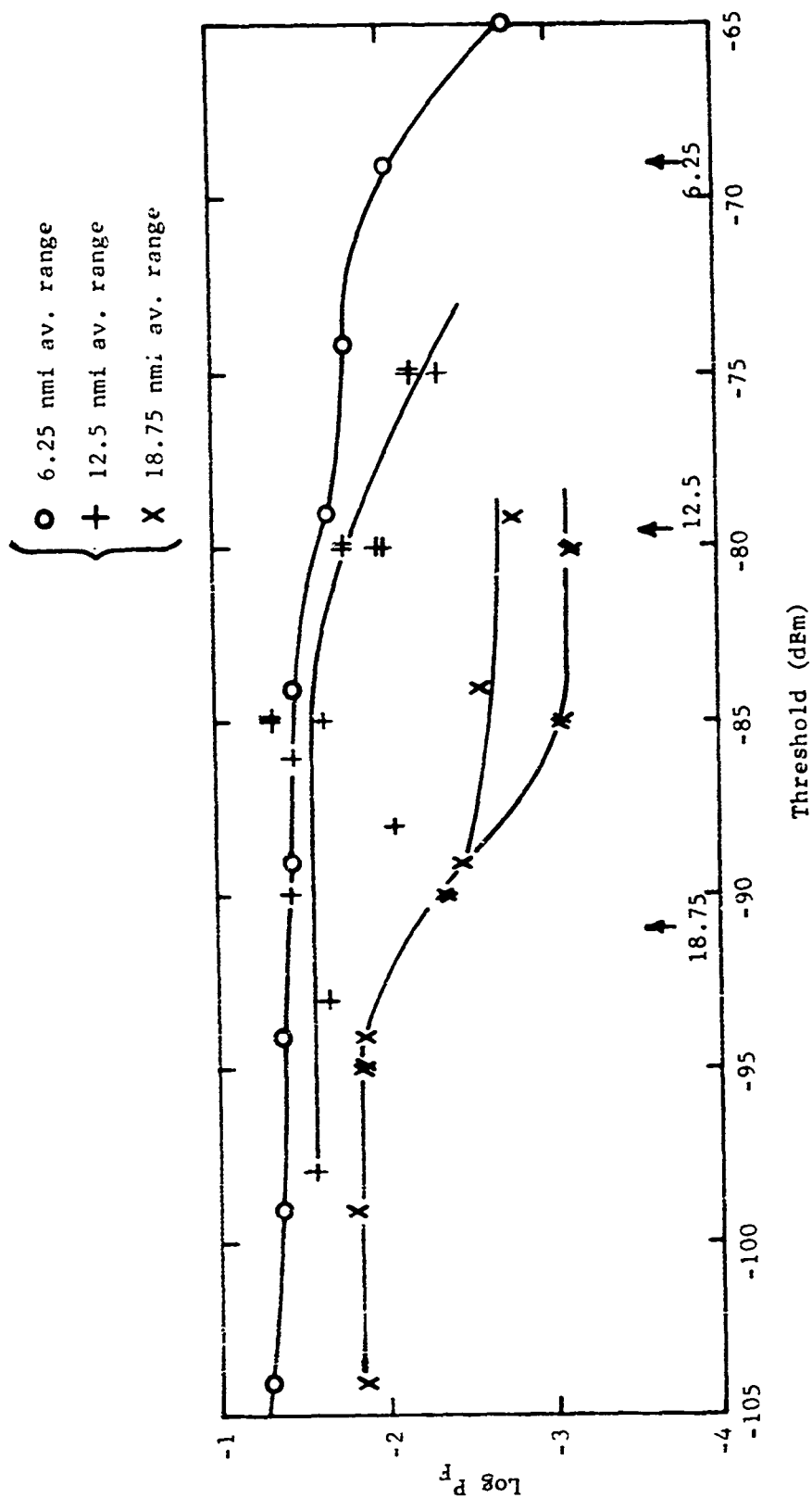


Figure 3. Probability of spike signal being above threshold received power. Arrows indicate estimated median spike levels at average ranges shown.

Table XI. Median Clutter Spike Cross Sections

<u>Displayed Range</u>	<u>Average Range</u>	<u>Cross Section</u>	<u>Number Dens</u>
10 nmi	6.25 nmi	-19 dBsm	$2.2/\text{nmi}^2$
20 nmi	12.5 nmi	-18 dBsm	$1.5/\text{nmi}^2$
30 nmi	18.75 nmi	-22 dBsm	$0.8/\text{nmi}^2$

It is difficult to decide on the basis of these data alone if the cross section of spikes should be considered as range independent, because such a conclusion would relate strongly to the definition of the propagation conditions that exist. Two minor comments can also be made about the data. There is a suggestion of two steps in the curve in Figure 3 for spikes at 6.25 nmi which suggests the existence of two spike mechanisms at that angle or on that day. Also, both the false-alarm rate (in radar space) and the number density (in map space) are monotonic decreasing functions of range.

The internal consistency of these data is considered to be good and the data are interpreted to be in support of the hypothesis that clutter spikes have well-defined cross sections.

The question of how a human operator reacts to such a clutter environment was investigated with the following described experiment. Radar PPI operators were assigned the task of designating detected targets in the 45° by 40% of displayed range area, and of investigating the signal strength of all detected targets by stopping the scanning antenna and measuring the signal on an A-scope. The experiment was performed in an area of ocean frequented by many transient boats of all sizes. It was found that out of about 25 targets detected, two were observed to have occasional peak signals about 10 dB above the median spike levels, none were detected with less than 10 dB peak-signal to median-spike ratio and all others were greater in peak strength. It is known that target signals were present but not detected in this experiment with peak strengths less than 10 dB above the spikes.

It is interesting to compare the above results with the thresholds for detection of target signals in noise. Assume that an operator will use a threshold equivalent to one producing a false-alarm number of about 10^4 (see Chapter IV) and that the temporal correlation of a spike is long compared to the dwell time of the antenna beam on a given azimuth, so that only one independent sample is obtained per scan. For these conditions the calculation displayed in Reference 10 for a non-fluctuating target predicts a signal-to-average-noise ratio of about 10 dB to achieve $P_D = 0.5$ which is consistent with the observed result. Thus it is concluded that a useful model is the noise model with the median spike level substituted for the average noise and only one pulse effectively integrated.

VI* ACKNOWLEDGEMENT


The experiments described in Chapter VI were carried out with the essential help of Robert Nester of Airtronics, Inc. The concepts developed in that Chapter were evolved in discussions with R. Nester and R. Hess of Airtronics, Inc. and F. Dyer of Georgia Tech. The participation and cooperation of operators from the Fleet Anti-air Warfare Training Center, San Diego, California, and personnel of Teledyne/Micronetics, Inc. are appreciated.

Submitted by

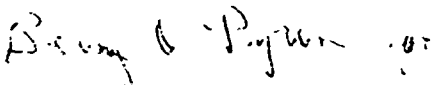


Wayne Rivers
Principal Research Physicist

Approved by



F. B. Dyer
Project Director



R. M. Goodman, Jr.
Head, Sensor Systems Branch

VIII. REFERENCES

1. A. V. Haeff, "Minimum Detectable Radar Signal and its Dependence Upon Parameters of Radar Systems," Proc. IRE 34 857 (1964)
2. R. Payne-Scott, "The Visibility of Small Echoes on Radar PPI Displays," Proc. IRE 36 180 (1948)
3. C. H. Baker, Man and Radar Displays, MacMillan (1962)
4. R. M. Boynton, C. Elworth, and R. M. Palmer, "Laboratory Studies Pertaining to Visual Air Reconnaissance," WADC Technical Report 55-304 Part III, April 1958, AD 142274
5. J. L. Lawson and G. E. Uhlenbeck, Threshold Signals, McGraw Hill (1949), Chap. 8
6. H. R. Blackwell, "Contrast Thresholds of the Human Eye" J.O.S.A. 36 624 (1946)
7. O. H. Schade, "An Evaluation of Photographic Image Quality and Resolving Power," J. Soc. Motion Picture and Tel. Engr. 73 81 (1964)
8. J. L. Marcum, "A Statistical Theory of Target Detection by Pulsed Radar," IRE Trans. IT-6 59 (Apr 1960)
9. P. Swerling, "Probability of Detection for Fluctuating Targets," IRE Trans. IT-6 269 (Apr 1960)
10. J. DiFranco and W. Rubin, Radar Detection, Prentice Hall (1968)
11. D. G. Tucker, "Detection of Pulse Signals in Noise: Trace-to-Trace Correlation in Visual Displays," J. Brit. IRE 17 319 (1957)
12. M. I. Skolnik, "Discussion: Trace-to-Trace Correlation in Visual Displays," J. Brit IRE 17 705 (1957)
13. S. B. Williams, "Visibility on Cathode-Ray Tube Screens: Viewing Angle," J.O.S.A. 39 782 (1949)
14. J. A. Swets and D. M. Green, "Sequential Observations by Human Observers of Signals in Noise," Signal Detection and Recognition by Human Observers John Wiley & Sons (1964)
15. K. R. Schmidt, "Statistical Time-Varying and Distribution Properties of High-Resolution Radar Echo," NRL Report 7150, Nov 1970.
16. W. Rivers, "Low Angle Radar Sea Return at 3-mm Wavelength," Final Report on Contract N62269-70-C-0489, 15 November 1970, Georgia Institute of Technology, AD 717 082
17. W. K. Rivers, S. P. Zehner, and F. B. Dyer, "Modeling for Radar Detection," Final Report on Contract N00024-69-C-5470, 31 December 1969, Georgia Institute of Technology, AD 507 375

IX. APPENDIX

A. Properties of a Curve-Fitting Function

Many occasions arise requiring a function with simple asymptotic properties and curvature in the transition region between the asymptotes. A useful example of a large family of functions is:

$$f(x) = (1 + x^p)^{\frac{1}{q}} \quad (8)$$

Its interesting properties are described by:

$$\text{for } x \ll 1, f(x) \approx 1; \quad (9)$$

$$\text{for } x \gg 1, f(x) \approx x^{\frac{p}{q}};$$

$$\text{at } x = 1, f(x) = 2^{\frac{1}{q}}; \text{ and } (x=1, f(x)=1) \text{ designates}$$

the intersection of the two asymptotes.

Three choices of exponents illustrate their control of the hardness or softness of the corner. Let $p=q$. Then, for $p = 0.5, 1$, and 2 , $f(1) = 4, 2$, and $\sqrt{2}$, respectively. The case for $p = -q = 2$ is the form for the frequency response of a single stage R-C low-pass filter, with x identified as the normalized frequency and $f(x)$ as the magnitude of the voltage transfer ratio.

The slope of the left-hand asymptote is adjustable in the function,

$$f(x) = x^r (1 + x^p)^{\frac{1}{q}}, \quad (10)$$

which is described by:

$$\text{for } x \ll 1, f(x) \approx x^r; \quad (11)$$

$$\text{for } x \gg 1, f(x) \approx x^{r + p/q};$$

$$\text{at } x = 1, f(x) = 2^{\frac{1}{q}}; \text{ and}$$

$(x=1, f(x)=1)$ designates the intersection of asymptotes.

Thus, if a function is desired that has asymptotes with left and right slopes of +1 and -1, respectively, and a sharp corner, appropriate choices of exponents might be:

$$\begin{aligned}r &= 1, \\p &= 4, \\q &= -2.\end{aligned}$$

A soft-corner function with the same slopes would result from:

$$\begin{aligned}r &= 1, \\p &= 1, \\q &= -\frac{1}{2}.\end{aligned}$$

B. Brief Summary of FOCAL Commands and Symbols

The summary of commands and symbols given in Table XII is intended to provide sufficient information for the qualitative understanding of the FCCAL programs listed in this report. The reader should consult the literature of the Digital Equipment Corporation if detailed use of the FOCAL language is contemplated.

XII. Selected FOCAL Commands and Symbols

<u>Symbols or Command</u>	<u>Abbreviation</u>	<u>Function</u>
SET	S	Sets the value of the variable following the command to that of the expression after the equals symbol
COMMENT	C	Program ignores following statement
GOTO	G	Transfers program to line number indicated
ASK	A	Requests a value of variables from the teletype
TYPE	T	Outputs the value of variables or statements to the teletype
DO	D	Performs the instructions of line or block indicated and returns program to next statement following DO
QUIT	Q	End of program
;		Separates statements on the same line
?		Causes teletype to type the enclosed characters as the statement is executed
+		Add
-		Subtract
*		Multiply
/		Divide
↑		Exponentiation (integer exponent only)
AA		A variable name; any two letters qualify

XII. Selected FOCAL Commands and Symbols (Continued)

<u>Symbols or Command</u>	<u>Abbreviation</u>	<u>Function</u>
FSQT(X)		Square root of X
FLOG(X)		Natural logarithm function ($\log_e X$)
FEXP(X)		Generates e to the power X
FSIN(X)		Generates the sine of X in radians
FOR	F	Performs statements following semi-colon on same line for values of the indicated variable: Start, Step, Last